YTUP

Journal of Thermal Engineering

https://jten.yildiz.edu.tr/

https://doi.org/10.47481/jten.0007

RESEARCH ARTICLE

Performance comparison evaluation and selection of optimal heat transfer fluid for parabolic trough collector

Ipsita Mishra[1,2], Pragyan Senapati[1], Mukundjee Pandey[3]

[1]Department of Mechanical Engineering, Institute of Technical Education & Research, ITER College Rd, Jagmohan Nagar, Bhubaneswar, Odisha, 751030, India

[2]School of Maritime Studies, Centurion University of Technology & Management, Ramachandrapur, Jatni, Bhubaneswar, Odisha, 751030, India

[3]Department of Mechanical Engineering, Centurion University of Technology & Management, Ramachandrapur, Jatni, Bhubaneswar, Odisha, 751030, India

Abstract

Background: The solar parabolic trough collector is among the most promising technologies for converting solar energy into useful thermal energy. Nevertheless, it needs better heat-transfer fluid to operate optimally. The main purposes of this study are to determine the thermal and hydraulic performance of a parabolic trough collector and compare four synthetic organic heat-transfer fluids, namely, Dowtherm-rp, Dowtherm-j, Syltherm-800, and Therminol-vp1. This work is special in its approach to the comparative performance analysis of four high temperature heat transfer fluids: Dowtherm-rp, Dowtherm-j, Syltherm-800 and Therminol-vp1 and the ability to infer the thermal performance of each fluid in terms of operating parameters. Techniques: In this study, computational fluid dynamics tools with a finite-volume capability and a Monte Carlo ray-tracing method that are implemented in ANSYS-AIM 2020R1 were used. The calculations and plotting of the parabolic trough collector heat transfer on the base of the mathematical formulation of the heat transfer are done using MATLAB R2020a with the help of Microsoft Excel. Accurate capturing of complex conjugate heat transfer, radiative effects and hydraulic behavior in the system is done using computational fluid dynamics. Both localized and overall system performance under different operating conditions can be assessed using mathematical formulation and analysis. Findings: The maximum pressure drops of 49.619 Pa and 43.712 Pa are in Dowtherm-rp and Dowtherm-j respectively at a value of the operating parameter of 0.20. Conversely, Syltherm-800 and Therminol-vp1 have greater convective heat transfer coefficient, 146.924 W/m^2-K and 173.726 W/m^2-K respectively. Interestingly, Syltherm-800 and Dowtherm-rp have a considerable heat loss of 2906.7 W and 2564.623 W, respectively, at the same conditions of operation. Inferences: Therminol-vp1 and Syltherm-800 had a thermal enhancement index of 1.254 and 1.0, respectively. Also, Syltherm-800 and Dowtherm-rp have the highest thermal efficiency of 0.367 and 0.451 respectively. All in all, Syltherm-800 will have the best thermal and hydraulic properties, making it the most suitable fluid as a heat transfer media.

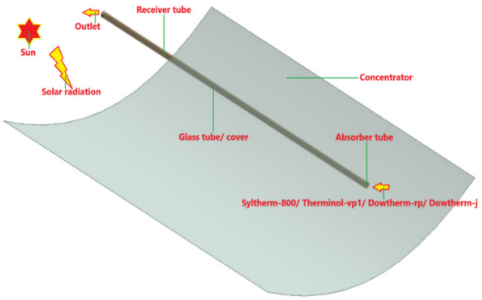

Keywords: Dowtherm-rp, Dowtherm-j, Syltherm-800, Therminol-vp1, thermal efficiency, thermal performance index

Cite this article as: Mishra, I., Senapati, P., & Pandey, M. (2026). Performance comparison evaluation and selection of optimal heat transfer fluid for parabolic trough collector. Journal of Thermal Engineering, 12(3), 2–14. https://doi.org/10.47481/jten.0007

*Corresponding Author
E-mail Adress: mukundjee.pandey@cutm.ac.in

Submitted: 15 July 2025; **Accepted:** 31 July 2025

This paper was recommended for publication in revised form by Editorin-Chief Ahmet Selim Dalkılıç

1. Introduction

The Introduction section examines whether fluid types and properties are important for evaluating the performance of parabolic trough collectors (PTCs). The LS-2 parabolic trough collector was investigated to determine the extent to which variations in plug diameter and position affected the outlet temperature and the overall system efficiency. The results showed that an optimum nondimensional displacement of 0.5 created a significant influence on thermal performance and this could be explained by the collective toxins of nonuniform distribution of heat flux and thermophysical diversity of the working fluid [1].

We start by evaluating the influence of utilization of base fluids in isolation, heat transfer fluids (HTFs) on the PTCs operation. Synthetic oil was used as the HTF to assess the optical performance of a PTC in Algeria with a maximum optical efficiency of 79.38. The study, which focused on the effect of geometric and optical properties on the performance of the system when subjected to the real-world weather conditions, revealed that the highest local concentration ratio of 116.30 was at the lower part of the receiver tube [2]. In this study, numerical exploration of the enhancement of heat transfer in PTCs using numerous twisted tape inserts using pressurized water as the working fluid was carried out. Although dual square cut twisted tapes exhibited a 16 and 12 % improvement in the thermal performance at Reynolds numbers, the findings showed that dual V-cut twisted tapes had a 19.58 and 17.44 % increase in the Nusselt number at Reynolds number of 10,000 and 20,000, respectively, respectively, compared to plain tubes [3]. The period 2015-2023 was devoted to the evaluation of the heat-transfer methods of parabolic-trough solar collectors, with special emphasis on the inserts in the form of twisted tapes or wire coils. Whereas porous metal foams enhanced thermal performance by 171.2 % over non-porous tubes at full porosity and 119.6 % at semi-porosity, wire-coiled inserts yielded better thermal performance results with 6-45 mm pitch distances, with square-cut versions showing the best thermal performance results [4].

The effects of metallic and nonmetallic nanoparticles dispersed in base fluids that are used as HTFs are examined. Subsequently, the emphasis was put on the heat transfer coefficient in the collector receiver tube with the addition of Al_2O_3/Oil nanofluid and a modified converging-diverging tube geometry leading to significant increases of 0.22 % and 1.13 % in thermal efficiency each [5]. A PTC based evacuated-tube collector was invented; it was able to warm water to temperatures of 40 to 68 with low solar irradiance. This system showed a 30 % higher heating efficiency but did not affect the thermal stability of the HTF, Therminol d-12, during 100 continuous operational cycles [6]. Metal-oxide nanofluids, such as CuO and CeO_2, have been considered thermal conductors in PTCs. The paper noted that the top level of heat loss reduction of up to 5.5 % by CuO nanoparticles was achieved by focusing on the effect of fluid properties and configurations of absorbers in performance [7]. More studies on the Dowtherm-a oil-based nanofluids were conducted to determine that the outlet temperatures and thermal efficiencies improved substantially with the addition of Au nanoparticles, with a reported efficiency of 50 % at high inlet velocities [8]. Research has shown that the PTC receiver experiences substantial heat losses, resulting in low thermal efficiency. Therefore, heat-transfer augmentation methods are necessary. An analytical model with an error of less than 5.5 % showed that combining Fe_3O_4/H_2O nanofluid with twisted-tape inserts increased the Nusselt number by up to 87 %, whereas the nanofluid or the inserts alone increased it by up to 59 %. The researchers concluded that the use of twisted tape in the form of water (H_2O) is the best way of enhancing thermal efficiency over the Reynolds number range tested [9]. Furthermore, the combination of a PTC with a single slope solar still proved that the employment of CuO/mineral oil nanofluid led to the inclusion of freshwater productivity by 71.2 % as opposed to conventional approaches [10]. An in-depth comparison of different HTFs of PTCs highlights the effectiveness of metal oxide hybrid nanofluids in improving thermal conductivity and system efficiency of working fluids that were essential in selecting the working fluid optimally [11].

System operations deserve to be compared with the effects of various liquid and gaseous HTFs. Water and steam, molten salts and pressurized gases were considered as working fluids in PTCs, but none of them turned out to be an ideal short-term solution since they had technical issues that were not resolved. As it was observed, future studies on new working fluids and especially development of cheaper thermal storage systems and new salt mixtures with lower melting points are important in improving the viability and efficiency of PTCs in the future [12]. Solar energy harnessed by the Eurotrough ET-150 PTC, is a versatile resource across a wide temperature range. Different working fluids, such as pressurized water, Therminol-vp1, molten nitrate salt, liquid sodium, air, carbon dioxide and helium were tested to establish the best mass flow rates. Liquid sodium achieved the highest exergetic efficiency of 47.48 % at 800 K, while pressurized water was best for temperatures up to 550 K, and carbon dioxide and helium were suitable for temperatures exceeding 1100 K [13]. Helium provided the highest exergetic efficiency at temperatures up to 700 K, whereas carbon dioxide did so at temperatures above 700 K. Air and nitrogen performed adequately, whereas argon performed less efficiently. To maximize the efficiency of PTCs, it was necessary to optimize the mass flow rate and minimize pressure drop [14].

Synthetic oils performed better than other HTFs in terms of thermal efficiency and thermal enhancement index. Also, the behavior of a PTC in a solar thermal power plant was simulated, which shows that therminol oil was more effective than other HTFs, with an extraction efficiency of 81.7 % [15]. Lastly, the supercritical carbon dioxide (s-CO2), Therminol-vp1 and molten salt were compared as HTFs of PTCs across different operating conditions. The lower cost of S-CO_2 and its ability to integrate with small scale storage systems enables it to provide economic gains although it has similar energy and exergy efficiencies as those of Therminol-vp1 and molten salt in the PTC. Molten salt was also better in terms of thermal energy

storage (TES) efficiency but Therminol-vp1 was much better in its volume capacity and only needed a third of the volume of the tank [16]. In this work, PTCs with Syltherm-800 and Therminol-vp1 as baseline fluids, both with metal-oxide nanoparticles, including CuO and CeO2, were compared. It was found that CuO/Therminol-vp1 nanofluids reached a peak heat loss drop of 5.5 % and thermal efficiency increased at an average rate of 5.1 % per 1 % volume fraction of nanoparticles [17]. This experiment examined the thermal characteristics of a PTC with synthetic oil/Cu nanofluids to determine their ability to improve the heat transfer of the body in different operating conditions. Results revealed that whereas synthetic oil/Cu nanofluids increased the convective heat transfer coefficient over a wide range of operating conditions, larger pressure drop required more pumping power [18]. Of all the thermal oils analyzed, we found that Therminol-vp1 with Al_2O_3 TiO2 had the highest mean thermal efficiency of 71.68, whereas Syltherm-800 Al_2O_3 TiO_2 had the highest exergy efficiency of 24.1 % [19].

Few studies compare the performance of synthetic oils in PTCs. The main objective of this research is to predict and compare the operational performance of parabolic trough collectors using four synthetic thermal fluids: Dowtherm-rp, Dowtherm-j, Syltherm-800, and Therminol-vp1. When selecting the HTFs for this study, we focused on those that are widely used and welldocumented in the literature, particularly for applications related to heat transfer in industrial systems.

This study uniquely focuses on the comparative performance of four high-temperature HTFs: Dowtherm-rp, Dowtherm-j, Syltherm-800, and Therminol-vp1. and inferring their individual thermal performances with respect to operating parameters (P_{op}).

The results indicate that Dowtherm-rp and Dowtherm-j exhibit the highest-pressure drops, 49.619 Pa and 43.712 Pa, respectively, at an operating parameter value of 0.20. Conversely, Syltherm-800 and Therminol-vp1 have a higher value of convective heat-transfer coefficient: 146.924 W/m^2-K and 173.726 W/m^2-K respectively. It is interesting to note that with the same operating conditions, Syltherm-800 and Dowtherm-rp have very high heat losses of 2906.7 W and 2564.623 W respectively. The thermal enhancement index of Therminol-vp1 and Syltherm-800 are 1.254 and 1.0, respectively. Syltherm-800 and Dowtherm-rp have the highest thermal efficiency of 0.367 and 0.451 respectively. Overall, Syltherm-800 is the most effective HTF, combining optimal thermal and hydraulic properties.

The present study uses geometric modelling to provide a detailed, dimensioned description of the PTC. Subsequently, the study generates meshes for both the solid and fluid domains and assesses mesh quality using a grid-independence test. After that the boundary condition and validation section proceeds with the setting of inlet, outlet and wall boundary conditions and validation of numerical simulation with Dudley et a. (1994) experimental findings. The next section presents detailed steps to formulate the mathematical solution for the numerical analysis required to obtain the desired results.

2. Geometric modelling

To conduct reliable computational fluid dynamics (CFD) simulations, it is crucial to develop precise three-dimensional geometries using computer-aided design tools. Figure 1 presents a model in which an absorber tube is enclosed by a glass envelope, creating a vacuum-insulated annular region between the tube and the envelope; the two together form the receiver assembly. The CAD model includes specific dimensions. The inner tube of the absorber ($D_{in,ab}$) has an internal diameter of 0.066 m, whereas the outer diameter of the absorber ($D_{ou,ab}$) is 0.070 m. The inner and outer diameter of the glass tube is 0.109 m and 0.115 m ($D_{in,gl}$) and ($D_{or,gl}$), respectively. The length (L)of the receiver tube is 7.8 m and the angle of the rim (φ) is 60 degrees. The parabolic trough collector (PTC) concentrator has a focal length (F_L)of 1.84 m, an aperture width (W_{ap}) of 5 m, and achieves a concentration ratio (Cr) of 22.74. They are defined by a selective coating which absorbs the solar radiation when coated on the outer surface of the absorber tube. To facilitate heat transfer, a heat transfer fluid (HTF) flows through the absorber tube at a specified mass flow rate and is aided by an external device that generates a pressure drop. The receiver tube is located at the focal line of a parabolic trough concentrator (PTC). The receiver-tube assembly used in the present study has a coaxial design, consisting of an inner cylindrical component, commonly known as the absorber tube, enclosed within an outer glass enclosure. The space between the two tubes is maintained under vacuum to minimize convective thermal losses in the system.

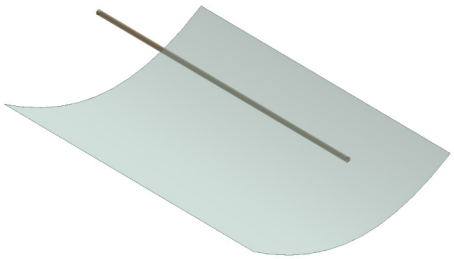

Figure 1. 3-Dimensional Computer Aided Design model of parabolic trough collector (PTC)

3. Meshing

Mesh generation and grid-independence validation are two important steps in computational fluid dynamics (CFD) simulations, particularly when characterizing two-way heat-exchange processes between the receiver tube and the heat transfer fluid (HTF) that flows through it. The meshing of two computational domains (solid and fluid) was done using tetrahedral elements, as illustrated in Figure 2. Though hexahedral meshes are less costly and more accurate at low

computational cost, they are inapplicable to complicated 3D models, so tetrahedra meshes are more viable even though they have a higher cost of computation.

The quality of mesh was considered through orthogonality (0.819) and skewness (0.179) as indicated in Table 1. A grid independence test determined an optimal mesh size of 0.0041 m, as shown in Table 2. As the number of elements increased, errors in $T_{ab,in,}$ and T_{ot} decreased. Base temperatures for $T_{ab,in,}$ and T_o were 526.190 K and 433.900 K, with errors of 0.4110 and 0.3950, respectively.

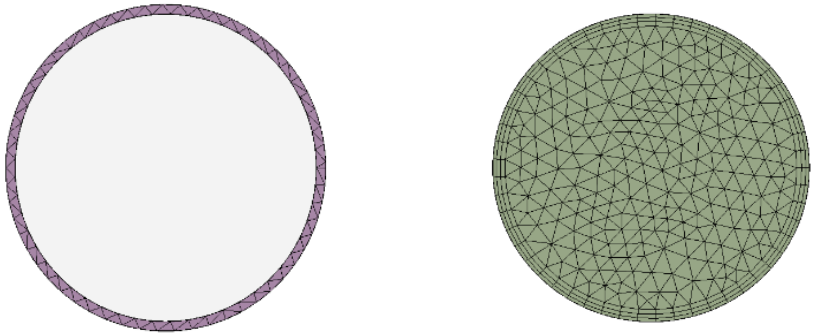

Figure 2. Tetrahedral meshing of solid and fluid domains

Table 1. Skewness and Orthogonality of mesh

Meshing Elements HTF/ absorber	Skewness HTF/ absorber	Orthogonality HTF/ absorber
1953870/465418	0.182/0.438	0.817/0.561
2331600/524847	0.181/0.403	0.818/0.596
2649644/573825	0.179/0.376	0.819/0.624
3036281/620620	0.179/0.355	0.819/0.644
3466564/677309	0.179/0.331	0.819/0.669
4080247/779463	0.179/0.305	0.819/0.695

Table 2. Grid independence test

Size (mm)	$T_{ab,in}$ (K)	$T_{ab,in,error}$	T_o (K)	$T_{o,error}$
0.0049	660.69	-1.161	414.20	-0.744
0.0047	660.45	-1.124	413.89	-0.669
0.0045	659.28	-0.945	413.86	-0.661
0.0043	657.79	-0.717	412.94	-0.438
0.0041	657.98	-0.746	412.93	-0.435
0.0039	653.11	base	411.14	base

4. Boundary conditions and validation

This simulation models two interacting domains: a solid receiver tube and the heat transfer fluid (HTF) inside it. The interaction between the surfaces is the coupling between the inner solid region and the external fluid boundary. The inlet and outlet boundary conditions are specified as mass flow rate and pressure (p), respectively, and the expressions and assumptions regarding their variations under fully developed flow conditions are stated in the foregoing discussion. The boundary conditions governing the simulation are defined as follows: at the inlet, the mass flow rate ranges between 0.2 kg/s and 1.2 kg/s; at the outlet, fully developed flow conditions are assumed, whereby the streamwise gradients of all dependent variables including velocity components (u, v, w), turbulent kinetic energy (k), turbulent dissipation rate (ε), pressure (p), and temperature (T) are set to zero, expressed as $\partial u/\partial x = \partial v/\partial x = \partial w/\partial x = \partial k/\partial x = \partial \varepsilon/\partial x = \partial p/\partial x = \partial T/\partial x = 0$; while the non-uniform heat flux applied to the lower lateral surface is determined through the Tonatiuh-2.2.4 simulation software. The wall heat-flux boundary conditions are adopted directly from the open-source ray-tracing software. The lower lateral surfaces receive concentrated solar radiation from the parabolic concentrator. The upper and lateral surfaces receive direct solar radiation and albedo radiation, respectively. The heat flux that is spread over the upper lateral surface is calculated using the Monte Carlo Ray Tracing (MCRT) which provides a calculated value of the product of direct beam irradiance and solar absorptivity and transmissivity which is expressed in the form of I_b. The lower lateral surface of the tube, bounded by the edge angle (∅) of the parabolic trough collector (PTC), absorbs the thermal flux, which was simulated using the Tonatiuh-2.2.4 MCRT method, as shown in Figure 3(a). Also, as indicated by Figure 3(b), the heat flux data generated by Tonatiuh-2.2.4 MCRT method has been validated with Hachicha et al. (2013) findings. Variables x and y denote the tube's outer diameter and length, respectively; θ° denotes the perimetric angle. The upper surface receives heat flux $I_{br} \times \alpha \times \tau$ (I_{br} solar radiation, α absorptivity, τ glass transmissivity). Side surfaces get 0.20 $\times I_b \times \alpha \times \tau$, and the tube ends are thermally adiabatic. The results of the CFD simulation were confirmed by experimental data obtained using nanofluids as the HTF, as detailed in Table 3.

Table 3. CFD data is validated against Dudley et al. (1994) experimental results [20].

Case No	I_{br} (W/	(kg/s)	T_i (K)	T_o (K) (Exp)	(K) (CFD)	(%) (Error)
1	933.7	0.6782	375.5	397.5	398.411	0.2291
2	968.2	0.6533	424	446	446.324	0.0726
3	928.3	0.7205	471	493	493.358	0.0726
4	909.5	0.81	524.2	542.9	543.509	0.1121
5	937.9	0.6253	570	589	589.205	0.0348
6	880.6	0.6209	572	590	590.193	0.0327
7	903.2	0.5682	628	647	647.252	0.0389
8	920.9	0.5434	652	671	671.371	0.0553

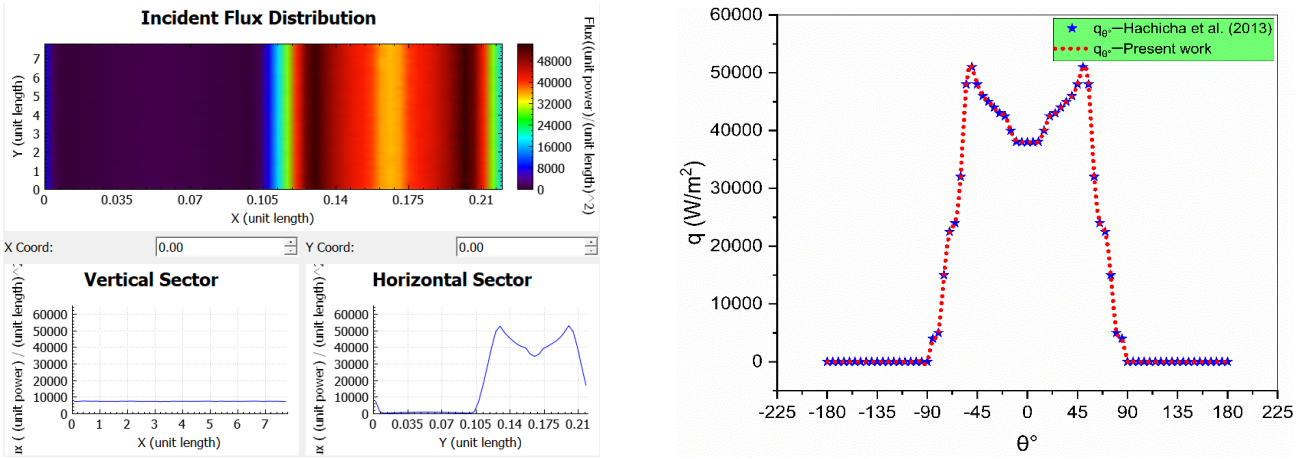

(a) **(b)**

Figure 3. (a) Flux distribution results from Tonatiuh-2.2.4.
(b)Simulated heat flux profile comparatively validated using the Tonatiuh 2.2.4 MCRT tool

5. Mathematical formulation

MATLAB R2020a and Microsoft Excel were used to perform calculations and generate plots based on the mathematical formulation of heat transfer in the parabolic trough collector (PTC). These calculations use input parameters based on the outcome of computational fluid dynamics (CFD) simulations and thus provide a precise and complete analysis of the system performance.

Energy received (Q_{er}) by the PTC is given by [21];

$$Q_{er} = A_{ap} \times I_{br} \quad (1)$$

where aperture width and beam radiation are denoted by A_{ap} and I_{br} respectively.

Heat gained (Q_{hg}) by the PTC can be expressed by;

$$Q_{hg} = \dot{m} \times C_p \times (T_o - T_i) \quad (2)$$

where the mass flow rate, specific heat, outlet temperature, and inlet temperature are denoted by $\dot{m}$, C_p, T_o, and T_i respectively.

The thermal efficiency () of the PTC is given by;

$$\eta_{th} = Q_{hg}/Q_{er} \quad (3)$$

Heat lost (Q_{loss}) by the PTC is given by;

$$Q_{loss} = \frac{A_{ou,\ ab} \times \sigma \times (T^4_{me,ab} - T^4_{me,gl})}{\frac{1}{\ _{se,ab}} + \frac{1 - \ _{gl}}{\ _{gl}}\left(\frac{D_{ou,\ ab}}{D_{in,gl}}\right)} \quad (4)$$

where the outer lateral area of absorber tube, Stefan Boltzmann constant, mean temperature of absorber tube, mean temperature of glass, absorber tube's emissivity, glass tube's emissivity, outer diameter of absorber tube, and inner diameter of glass tube are denoted by $A_{ou,ab}$, σ, $T_{me,ab}$, $T_{me,gl}$, $\varepsilon_{se,ab}$, ε_{gl}, $D_{ou,ab}$, and $D_{in,gl}$ respectively.

The Nusselt number is given by [22];

$$Nu = (h_{in,ab} \times D_{in,ab})/k \quad (5)$$

where the Nusselt number, convective heat transfer coefficient in the inner lateral surface of the absorber tube, inner diameter of absorber tube, and thermal conductivity of HTF are denoted by Nu, $h_{in,ab}$, $D_{in,ab}$, and k respectively.

The convective heat transfer coefficient ($h_{in,ab}$) is given by [23];

$$h_{in,ab} = \frac{Q_{hg}}{(\pi \times D_{in,ab} \times L) \times (T_{in,ab} - T_{me,\ HTF})} \quad (6)$$

where the inner diameter of absorber tube, length of the absorber tube, temperature of inner lateral surface of absorber tube, and mean temperature of HTF are denoted by $D_{in,ab}$, L, $T_{in,ab}$, and $T_{me,HTF}$ respectively.

The friction factor is given by;

$$f = \frac{(\ \ p/L) \times D_{in,ab}}{\rho \times v_i^2/2} \quad (7)$$

where pressure drop, inner diameter of absorber tube, density, and inlet velocity of HTF are denoted by Δp, $D_{in,\ ab}$, ρ, and v_i respectively.

The thermal enhancement index is given by [24];

$$TEI = \frac{(Nu/Nu_0)}{(f/f_0)^{1/3}} \quad (8)$$

where $(Nu/\ Nu_0)$ and $(f/\ f_0)^{1/3}$ denotes the thermal performance and hydraulic performance respectively.

The operating parameter (P_{op}) is given by;

$$P_{op} = \frac{(T_i - T_{at})}{I_{br}} \quad (9)$$

where inlet temperature of HTF, atmospheric temperature, and beam radiation are denoted by T_i, T_{at}, and I_{br} respectively.

6. Solution formation

The governing mathematical equations presented in Table 4 are discretized using the finite-volume method (FVM)and solved with the computational fluid dynamics (CFD) software ANSYS AIM 2020 R1. During discretization, the temperature-dependent thermophysical properties of heat transfer fluids (HTFs) are incorporated into the CFD model and presented in Table 5. To handle pressure-velocity coupling, the SIMPLEC algorithm is employed, and a coupled boundary condition is applied at the solid-fluid interface. Convective terms of momentum and turbulent kinetic energy are discretized using the QUICK scheme, while pressure and gradient terms are discretized using the PRESTO scheme. Additionally, the UPWIND scheme, which is second order-accurate, is used to discretize both the energy and discrete-ordinate equations. The convergence criteria are set with a maximum residual of less than 10^{-6} for continuity, velocity, k, and ε variables, and less than 10^{-7} for energy-related equations.

Table 4. Governing equations with formulation

Equation's name	Formulation
Continuity	$\nabla \cdot (\rho V) = 0$
Momentum	$\nabla \cdot (\rho VV) = -\nabla p + \nabla \cdot \bar{\bar{\tau}} + \rho g$
Energy	$\nabla \cdot (\rho V C_p T) = \nabla \cdot (k \nabla T)$
Turbulent kinetic energy (k)	$\nabla \cdot (\rho kV) = \nabla \cdot \left[\left(\mu + \frac{\mu_t}{\sigma_k}\right) \nabla (k)\right] + G_k - \rho\epsilon,$ (where $\mu_t = C_\mu \rho \frac{k^2}{\epsilon}, \sigma_\epsilon = 1.3$)
Dissipation (ε)	$\nabla \cdot (\rho\epsilon V) = \nabla \cdot \left[\left(\mu + \frac{\mu_t}{\sigma_\epsilon}\right) \nabla (\epsilon)\right] + \frac{\epsilon}{k}(C_{1\epsilon} G_k - C_{2\epsilon} \rho\epsilon),$ (where $C_\mu = 0.09, \sigma_k = 1.0$)

Table 5. Thermophysical properties of heat transfer fluids (HTFs)

Thermophysical properties	Temperature dependent properties of HTFs
	Syltherm-800
Density (kg/ m^3)	$\rho = 1.38820 \times 10^{-6} T_i^2 - 1.02631570 T_i + 1.360 \times 10^3$
Thermal conductivity (W-m-K)	$k = -0.575340 \times 10^{-3} T_i^2 - 1.87520 \times 10^{-4} T_i + 0.190020$
Specific heat (J/kg-K)	$C_p = 0.17080 \times 10 T_i + 0.110770 \times 10^4$
Dynamic viscosity (Pa. s)	$\mu = 6.6720 \times 10^{-13} T_i^4 - 0.15660 \times 10^{-8} T_i^3 + 0.138820 \times 10^{-5} T_i^2 - 0.554120 \times 10^{-3} T_i + 0.848660 \times 10^{-1}$
	Therminol-vp1
Density (kg/ m^3)	$\rho = -2.3793 \times 10^{-6} T_i^3 + 2.737 \times 10^{-3} T_i^2 - 1.8711 T_i + 1.4386 \times 10^3$
Thermal conductivity (W-m-K)	$k = 1.0614 \times 10^{-11} T_i^3 - 1.9368 \times 10^{-7} T_i^2 + 2.0353 \times 10^{-5} T_i + 1.4644 \times 10^{-1}$
Specific heat (J/kg-K)	$C_p = 4.394 \times 10^{-9} T_i^4 + 7.7663 \times 10^{-6} T_i^3 + 4.9862 \times 10^{-3} T_i^2 - 1.1017 \times 10^{-1} T_i + 2.125 \times 10^2$
Dynamic viscosity (Pa.s)	$\mu = 1.6543 \times 10^{-19} T_i^4 - 3.9844 \times 10^{-16} T_i^3 + 3.617 \times 10^{-9} T_i^2 - 1.406 \times 10^{-10} T_i + 2.3165 \times 10^{-11}$
	Dowtherm-rp
Density (kg/ m^3)	$\rho = -0.7 T_i + 1.20631 \times 10^3$
Thermal conductivity (W-m-K)	$k = 6.38298 \times 10^{-8} T_i^2 + 4.14617 \times 10^{-5} T_i + 1.44376 \times 10^{-1}$
Specific heat (J/kg-K)	$C_p = 3.8487 T_i + 3.70586 \times 10^2$
Dynamic viscosity (Pa.s)	$\mu = -1.72269 \times 10^{-11} T_i^3 + 2.10514 \times 10^{-8} T_i^2 - 8.59503 \times 10^{-6} T_i + 1.17425 \times 10^{-3}$
	Dowtherm-j
Density (kg/ m^3)	$\rho = -1.48604 T_i + 1.26275 \times 10^3$
Thermal conductivity (W-m-K)	$k = 1.53862 \times 10^{-7} T_i^2 - 4.7654 \times 10^{-4} T_i + 2.4464 \times 10^{-1}$
Specific heat (J/kg-K)	$C_p = 6.41413 T_i + 01.00229 \times 10^3$
Dynamic viscosity (Pa.s)	$\mu = 1.26332 \times 10^{-10} T_i^3 - 1.25872 \times 10^{-7} T_i^2 + 4.21509 \times 10^{-5} T_i - 4.77447 \times 10^{-3}$

7. Results and discussion

The simulation results have been arrived at by taking into account the mass flow rate () of 0.4 kg/s, with ambient temperature (T_{am}) of 300.15 K and at airflow velocity ($V_{ou,gl}$) of 1m/s. Operating conditions for temperature and pressure in the simulations were adopted from the Bureau of Indian Standards (BIS), while air velocity was adopted from ISO 2533. The uncertainties of the simulation in terms of T and η_{th} error can be inferred from the Figure 4(a) and Figure 4(b) which are found to be 0.0231 and 0.105 respectively.

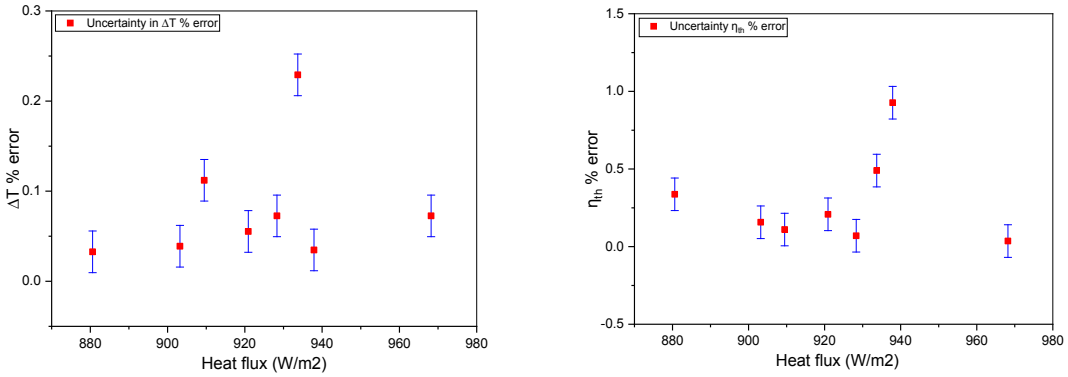

(a) **(b)**

Figure 4. (a) Variation of uncertainty in terms of T % error with heat flux. (b)Variation of uncertainty in terms of η_{th} error with heat flux

7.1. Effects of pressure

Figure 5 reveals that as the operating parameter (P_{op}) rises, the pressure drop(Δp) tends to rise for all heat transfer fluids (HTFs), excluding Syltherm-800, which exhibits a different behaviour. The value of p for Syltherm-800, and Therminol-vp1, Dowtherm-rp, Dowtherm-j decreases from 42.102 Pa to 28.197 Pa and increases from 24.451 Pa to 39.083 Pa, 36.743 Pa to 95.679 Pa, 16.035 Pa to 116.058 Pa respectively with an increase in P_{op} from 0.10 to 0.30. It occurs because the rise in P_{op} leads to a decrease in ambient temperature (T_{am}) or solar beam radiation (I_{bm}) values. Therefore, it indirectly increases the HTF's relative mean inlet temperature (T_{in}). This decrease or increase in with P_{op} is only related to the change in viscosity with T_{in} of the HTF. The viscosity for all other HTFs increases except for Syltherm-800 with rise in T_{in} and P_{op}. A decrease in viscosity reduces obstruction to HTF flow, whereas an increase exacerbates obstruction.

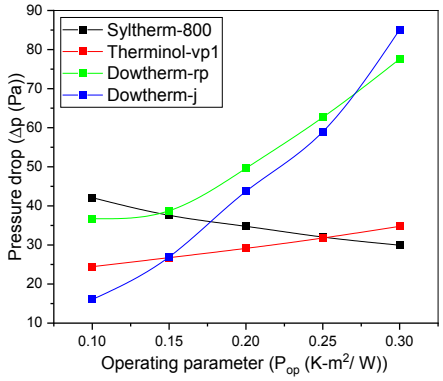

Figure 5. Variation of pressure drop (p) with operating parameters (P_{op})

7.2. Effects of convective heat transfer coefficient

As illustrated in Figure 6, increasing the operating parameter (P_{op}) results in a decline in the convective heat transfer coefficient(h)for all HTFs, except for Syltherm-800. The value of h for Syltherm-800, and Therminol-vp1, Dowtherm-rp, Dowtherm-j increases from 67.407 W/m^2-K to 230.895 W/m^2-K and decreases from 312.674 W/m^2-K to 78.599 W/m^2-K, 143.616 W/m^2-K to 118.623 W/m^2-K, 355.472 W/m^2-K to 26.115 W/m^2-K respectively with an increase in P_{op} from 0.10 to 0.30. As stated earlier, the viscosity and hence the density of the Syltherm-800 decreases while it increases for all other HTFs with an increase in T_{in}. This increase in viscosity enhances bulk molecular motion and increases h in Syltherm-800. Alternatively, a decrease in the viscosity, and hence the density, of Therminol-vp1, Dowtherm-rp, and Dowtherm-j results in reduced bulk molecular movement and, therefore, a decrease in h.

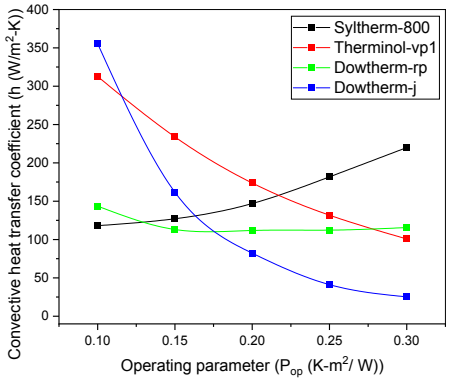

Figure 6. Variation of convective heat transfer coefficient (h) with operating parameters (P_{op})

7.3. Effects of heat loss

As shown in Figure 7, an increase in the operating parameter (P_{op}) leads to a rise in heat loss (Q_{loss}) across all heat transfer fluids (HTFs). However, the causes of the rise of Q_{loss} are different for Syltherm-800 and other HTFs. The value of Q_{loss} for Syltherm-800, Therminol-vp1, Dowtherm-rp, Dowtherm-j increases from 1637.4 W to 6490.1 W, 238.016 W to 3316.084 W, 357.130 W to 6988.879 W, and 95.151 W to 999900.345 W respectively with an increase in P_{op} from 0.10 to 0.30.

The value of Q_{loss} for Syltherm-800 increases due to enhancement in h and, hence, the heat transfer rate through the lower lateral surface of the absorber tube and, therefore, causes the enhancement of Q_{loss} from the upper lateral surface of the absorber tube. For other HTFs, the increase in Q_{loss} occurs due to a reduction in h and, hence, the increase of radiation heat losses.

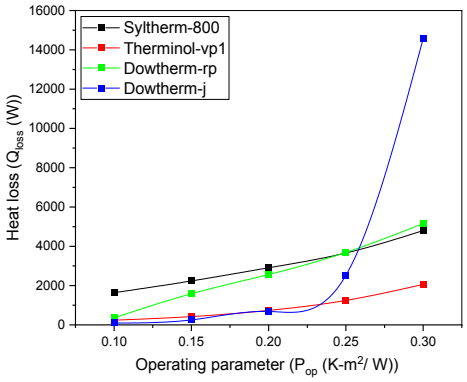

Figure 7. Variation of heat loss (Q_{loss}) with operating parameters (P_{op})

7.4. Effects of thermal enhancement index

As depicted in Figure 8, an increase in the operating parameter (P_{op}) results in a reduction in the thermal enhancement index (TEI)for all heat transfer fluids (HTFs), except for Syltherm-800. The conventional parabolic trough collector (PTC)with Syltherm-800 which is validated with Dudley et al. (1994) findings has been selected as a reference to determine TEI. Now, referring from the mathematical equations 8 and 9 it can be perceived that for all values of P_{op}, the value of TEI = $(Nu/Nu_0)/ (f/f_0)^{1/3}$ for Syltherm-800 remains "1" that is a constant. Assuming the ratio of the thermal and hydraulic performance of the Syltherm-800 as 1, the value of TEI for Therminol-vp1, Dowtherm-rp, Dowtherm-j decreases from 3.175 to 0.281, 1.273 to 0.315, and 1.421 to 0.065 respectively with an increase in P_{op} from 0.10 to 0.30. This occurs because for all HTFs except Syltherm-800, hydraulic performance overrides thermal performance in the PTC.

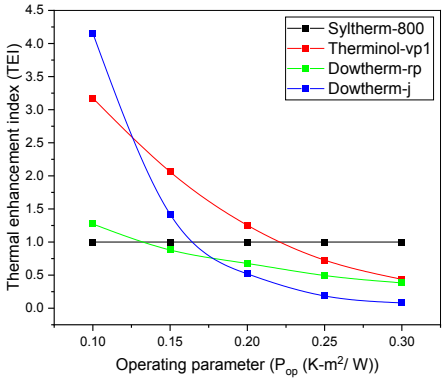

Figure 8. Variation of thermal enhancement index (TEI) with operating parameters (P_{op})

7.5. Effects of thermal efficiency

It can be seen from Figure 9 that with an increase in the operating parameter (P_{op}), the thermal efficiency(η)for all heat transfer fluids (HTFs)increases except for Syltherm-800 and Therminol-vp1. But the highest values of η for all values of P_{op} are shown by Dowthem-rp and Syltherm-800. The value of η for Syltherm-800, Therminol-vp1, and Dowtherm-rp, Dowtherm-j decreases from 0.3941 to 0.3472, 0.419 to 0.158 and increases from 0.306 to 0.442, 0.132 to 0.719, respectively with an increase in P_{op} from 0.10 to 0.30. This happens because, with an increase in P_{op}, the viscosity of Therminol-vp1, Dowthem-rp, and Dowthem-j leads to an increase. This decreases the velocity and increases the residence time of the HTF. This increase in residence time enhances the heat gained by the HTF per unit of heat acquired by the PTC. However, this is not the case for Therminol-vp1, because the increase in viscosity is insufficient to lengthen the HTF residence time. Also, the value of h for it is seen to be decreasing with increase in P_{op}; therefore, the η of Therminol-vp1 is decreasing.

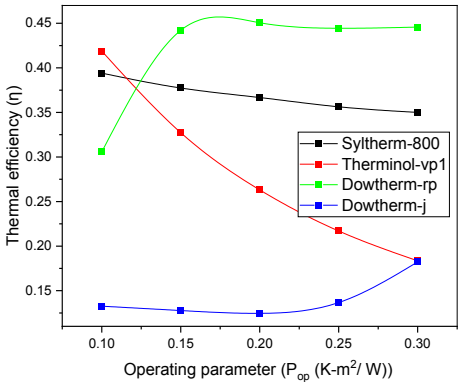

Figure 9. Variation of thermal efficiency(η) with operating parameters (P_{op})

7.6. Comparative performance

Among the evaluated heat transfer fluids (HTFs), Therminol-vp1 and Syltherm-800 exhibit the highest thermal enhancement index values of 1.254 and 1.0, respectively, at an operating pressure of 0.20.

Syltherm-800 and Dowtherm-rp also exhibit the highest thermal efficiencies under identical operating conditions, with values of 0.367 and 0.451, respectively. HTF outlet temperatures decrease in the following order: Dowtherm-rp, Syltherm-800, Therminol-vp1, and Dowtherm-j. Notably, the outlet pressures follow the same pattern as the temperature profiles, indicating a direct correlation between them. These observations are consistent with the temperature contours presented in Figures 10(a), 10(c), 10(e), and 10(g), and with the corresponding pressure contours shown in Figures 10(b), 10(d), 10(f), and 10(h).

The maximum outlet temperatures for Dowtherm-rp, Syltherm-800, Therminol-vp1, and Dowtherm-j are 885.59 K, 692.38 K, 678.18 K, and 468.61 K, respectively. Similarly, the maximum outlet pressures were 51.9 Pa, 30.387 Pa, 28.885 Pa, and 16.078 Pa. Table 6 can be used to deduce the sequences of outlet temperature and pressure contours of these HTFs.

Despite the Dowtherm-rp being more thermal efficient than Syltherm-800, Syltherm-800 has a balanced performance based on the measurements of thermal enhancement and hydraulic efficiency, thus, qualifies as the most versatile and effective HTF.

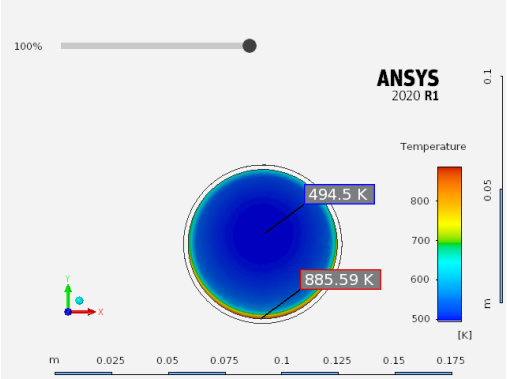

(a)

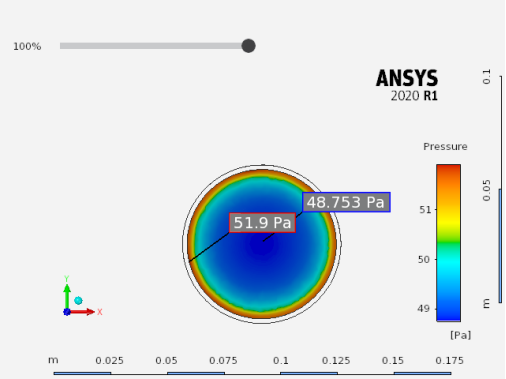

(b)

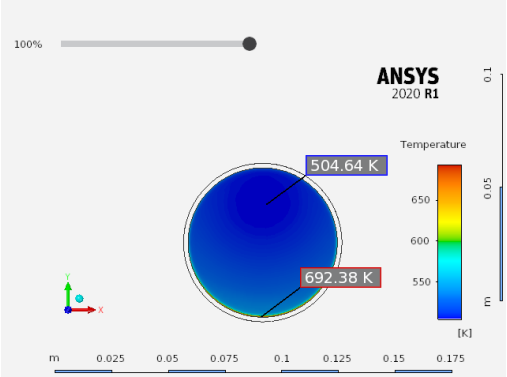

(c)

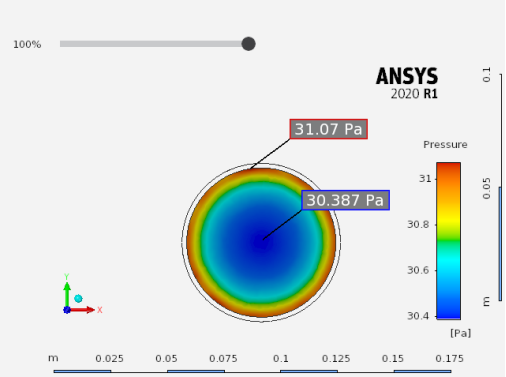

(d)

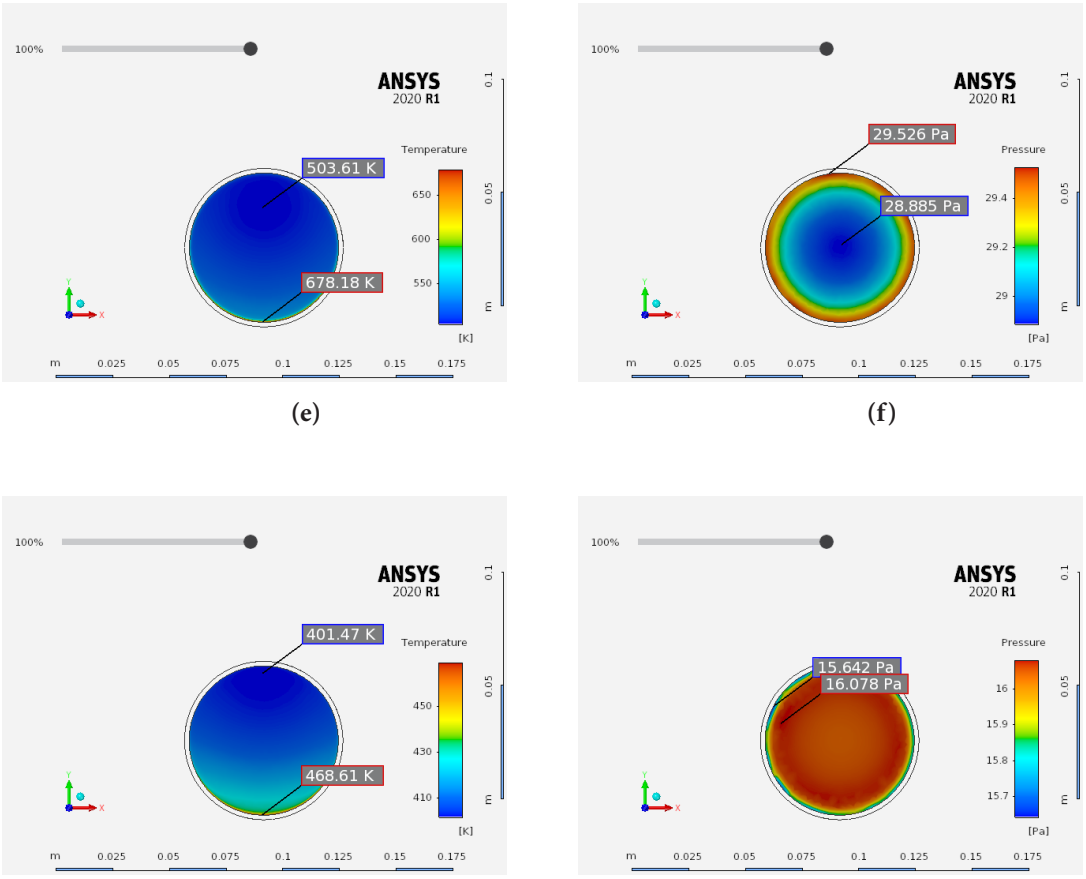

(e) **(f)**

(g) **(h)**

Figure 10. **(a)** Temperature contour of Dowtherm-rp. **(b)** Pressure contour of Dowtherm-rp. **(c)** Temperature contour of Syltherm-800. **(d)** Pressure contour of Syltherm-800. **(e)** Temperature contour of Therminol-vp1. **(f)** Pressure contour of Therminol-vp1. **(g)** Temperature contour of Dowtherm-j. **(h)** Pressure contour of Dowtherm-j.

Table 6. Variation of outlet temperature and pressures of HTFs

HTFs	Temperature (K)		Pressure (Pa)	
Sequence	Maximum	Minimum	Maximum	Minimum
Dowtherm-rp	885.59	494.5	51.9	48.753
Syltherm-800	692.38	504.64	31.07	30.387
Therminol-vp1	678.18	503.61	29.526	28.885
Dowtherm-j	468.61	401.47	16.078	15.642

8. Conclusion

This paper is a comparative analysis of four high temperature heat-transfer fluids, i.e. Dowtherm-rp, Dowtherm-j, Syltherm 800 and Therminol-vp1, with a focus on the thermal performance of each under different operating conditions and the unique performance features each exhibit.

Dowtherm-rp and Dowtherm-j are the highest pressure drop fluids that were evaluated in the heat-transfer. Dowtherm-rp and Dowtherm-j have pressure drops at an operating parameter value of 0.20 of 49.619 Pa and 43.712 Pa, respectively.

Syltherm-800 and Therminol-vp1 have better convective heat-transfer coefficients. With the same value of operating parameter, Syltherm-800 has a coefficient of 146.924 W/m^2-K and Therminol-vp1 has a coefficient of 173.726 W/m^2-K.

Syltherm-800 and Dowtherm-rp have the greatest values of heat loss. Syltherm-800 and Dowtherm-rp have heat losses at an operating parameter of 0.20, which are 2906.7 W and 2564.623 W, respectively.

Thermal enhancement indices are also found to be the greatest with Therminol-vp1 and Syltherm-800 with 1.254 and 1.0 respectively at an operating parameter of 0.20.

Also, Syltherm-800 and Dowtherm-rp have the highest thermal efficiencies. The efficiencies of syltherm-800 and Dowtherm-rp are 0.367 and 0.451 respectively as indicated in the temperature contours in Figure 10.

According to the overall thermal and hydraulic performance, Syltherm-800 is the best heat transfer fluid when compared to other analysed fluids.

Further research is underway to look at different nanoparticles to determine their effects on thermal performance of a geometrically optimised parabolic-trough solar collector.

The findings of this study can be applied to the design of solar thermal power generation systems and to industrial and process heating applications.

Nomenclature

A	Area (m^2)
C_p	Specific heat (J/kg. K)
CFD	Computational fluid dynamics
Cr	Concentration ratio
$C_1\varepsilon$	Empirical constant in ε-equation (1.44)
$C_{2\varepsilon}$	Empirical constant in ε-equation (1.92)
$C_{2\mu}$	Empirical constant for turbulence model
D	Diameter (m)
f	Friction factor
FL	Focal length (m)
g	Gravitational acceleration vector (m/s^2)
Gk	Turbulent kinetic energy (W/kg or m^2/s^3)
h	Heat transfer coefficient (W/m^2-K)
HTF	Heat transfer fluid
k	Thermal conductivity (W/m-K)
L	Length (m)
$\dot{m}$	Mass flow rate (kg/s)
Nu	Nusselt number
P	Parameter
p	Pressure
PTC	Parabolic trough collector
Q	Heat energy (W)
T	Temperature (K)
TEI	Thermal enhancement index
u	x component velocity (m/s)
v	y component velocity (m/s)
V	Velocity magnitude (m/s)
w	z component velocity (m/s)
x	x coordinate
y	y coordinate
z	z coordinate

Subscripts

ap	Aperture
ab	Absorber
at	Atmospheric
br	Beam radiation
gl	Glass tube
hg	Heat gained
i	Inlet
in	Inner
me	Mean
o	Outlet
0	Reference to standard
ou	Outer
se	Selective
th	Thermal

Greek Symbols

σ	Stefan's Boltzmann constant (W/m^2-K^4)
σ_ε	Turbulent Prandtl number for ε
σ_k	Turbulent Prandtl number for k
ρ	Density (kg/m^3)
ε	Emissivity
η	Thermal efficiency
τ	Transmissivity
k	Turbulent kinetic energy (m^2/s^2)
ε	Turbulent dissipation rate (m^2/s^3)
μ	Dynamic viscosity of the fluid (Pa·s)
μ_t	Turbulent (eddy) viscosity (Pa·s)
∇	Gradient operator
$\nabla\bullet$	Divergence operator
$\nabla()$	Gradient of a scalar or vector field

Authorship contributions

Ipsita Mishra: Conceptualization, Formal analysis, Validation, Data curation, Investigation, Writing-original draft. Pragyan Senapati: Methodology, Formal analysis, Supervision, Writing-review and editing. Mukundjee Pandey: Conceptualization, Software, Validation, Formal analysis.

Data availability statement

All data generated or discussed during this research are included in the published article. Supplementary raw data related to the reported results may be obtained from the corresponding author upon reasonable request.

Conflict of interest

The authors affirm that there are no known conflicting financial interests or personal associations that might have influenced, or could be alleged to have influenced, the results and conclusions presented in this manuscript.

Ethics

No ethical issues are associated with this manuscript.

Statement of the use of artificial intelligence

The authors confirm that they did not use any artificial intelligence tools to conceive, prepare, write, or edit this article. The work is solely that of the authors.

Funding

The author(s)reported that no funding was associated with the work featured in this article.

Copyright and permission statement

All figures included in this manuscript are the authors' original work.

References

[1] Sadaghiyani KO, Pourmahmoud N, Mirzaee I. Numerical simulation coupled with MCRT method to study the effect of plug diameter and its position on outlet temperature and the efficiency of LS-2 parabolic trough collector. ASME J Sol Energy Eng 2013;135(4):041001. doi:10.1115/1.4024475.

[2] Ghodbane M, Boumeddane B, Hussein AK, Li D, Sivasankaran S. Optical numerical investigation of a solar power plant of parabolic trough collectors. J Therm Eng 2021;7(3):550–69.

[3] Afsharpanah F, Sheshpoli AZ, Pakzad K, Ajarostaghi SSM. Numerical investigation of non-uniform heat transfer enhancement in parabolic trough solar collectors using dual modified twisted-tape inserts. J Therm Eng 2021;7(1):133–47.

[4] Raval P, Ramani B. Heat transfer enhancement techniques using different inserts in absorber tube of parabolic trough solar collector: A review. J Therm Eng 2023. doi:10.14744/thermal.0000847.

[5] Okonkwo EC, Abid M, Ratlamwala TAH. Numerical analysis of heat transfer enhancement in a parabolic trough collector based on geometry modifications and working fluid usage. ASME J Sol Energy Eng 2018;140(5):051009. doi:10.1115/1.4040076.

[6] Selvakumar P, Somasundaram P, Thangavel P. Performance study on evacuated tube solar collector using Therminol D-12 as heat transfer fluid coupled with parabolic trough. Energy Convers Manag 2014; 85:505–10. doi: 10.1016/j.enconman.2014.05.069.

[7] Brahim T, Jemni A. Comparative study of parabolic trough solar collector using Syslterm-800 and Therminol-VP1 non-metallic nanofluids. Therm Sci Eng Prog 2023; 43:101951. doi: 10.1016/j.tsep.2023.101951.

[8] Talem N, Mihoub S, Boumia L, Safa A, Navas J, Estellé P, Benayad Z. Thermal performance of parabolic trough collector using oil-based metal nanofluids. Appl Therm Eng 2024; 256:124128. doi: 10.1016/j.applthermaleng.2024.124128.

[9] Bilal FR, Arunachala UC, Sandeep HM. Experimental validation of energy parameters in parabolic trough collector with plain absorber and analysis of heat transfer enhancement techniques. J Phys Conf Ser 2018; 953:012030. doi:10.1088/1742-6596/953/1/012030.

[10] Nabil T, Dawood MMK. Numerical and experimental investigation of parabolic trough collector with focal evacuated tube and different working fluids integrated with single slope solar still. Heat Transfer 2020;50. doi:10.1002/htj.21966.

[11] Sarangi A, Sarangi A, Sahoo SS, et al. A review of different working fluids used in the receiver tube of parabolic trough solar collector. J Therm Anal Calorim 2023; 148:3929–54. doi:10.1007/s10973-023-11991-y.

[12] Zarza Moya E. Innovative working fluids for parabolic trough collectors. In: Blanco MJ, Ramirez Santigosa L, editors. Advances in concentrating solar thermal research and technology. Woodhead Publishing, 2017. p. 75–106. doi:10.1016/B978-0-08-100516-3.00005-8.

[13] Bellos E, Tzivanidis C, Antonopoulos KA. A detailed working fluid investigation for solar parabolic trough collectors. Appl Therm Eng 2017; 114:374–86. doi: 10.1016/j.applthermaleng.2016.11.201.

[14] Bellos E, Tzivanidis C, Antonopoulos KA, Daniil I. The use of gas working fluids in parabolic trough collectors – an energetic and exergetic analysis. Appl Therm Eng 2016;109(A):1–14. doi: 10.1016/j.applthermaleng.2016.08.043

[15] Kannaiyan S, Bokde ND. Performance of parabolic trough collector with different heat transfer fluids and control operation. Energies 2022; 15:7572. doi:10.3390/en15207572.

[16] Alaidaros AM, AlZahrani AA. Thermal performance of parabolic trough integrated with thermal energy storage using carbon dioxide, molten salt, and oil. J Energy Storage 2024; 78:110084. doi: 10.1016/j.est.2023.110084.

[17] Dou L, Ding B, Zhang Q, Kou G, Mu M. Numerical investigation on the thermal performance of parabolic trough solar collector with synthetic oil/Cu nanofluids. Appl Therm Eng 2023; 227:120376. doi: 10.1016/j.applthermaleng.2023.120376.

[18] Brahim T, Jemni A. Comparative study of parabolic trough solar collector using syslltherm-800 and therminol-VP1 non-metallic nanofluids. Therm Sci Eng Prog 2023; 43:101951. doi: 10.1016/j.tsep.2023.101951.

[19] Alhamayani A, Al-lehaibi M. The effect of adding hybrid nanoparticles (Al_2O_3–TiO_2) on the performance of parabolic trough solar collectors using different thermal oils and molten salts. Case Stud Therm Eng 2024; 59:104593. doi: 10.1016/j.csite.2024.104593.

[20] Dudley VE, Kolb GJ, Solan M, Kearney D. Test results: SEGS LS-2 solar collector. Sandia National Laboratories, 1994. Report No.: SAND94-1884, Albuquerque.

[21] Pandey M, Padhi BN, Mishra I. Numerical simulation of solar parabolic trough collector with viscous dissipation in slits of arc-plug insertion. Sol Energy 2021; 230:810–24. doi: 10.1016/j.solener.2021.11.008.

[22] Pandey M, Padhi BN, Mishra I. Numerical simulation of solar parabolic trough collector with arc-plug insertion. Energy Sources Part a Recover Util Environ Eff 2020;43(21):2635–55. doi:10.1080/15567036.2020.1822467.
[23] Mishra I, Senapati P, Pandey M. Numerical simulation of solar parabolic trough collector with twisted tape insertion shielded within inner cylindrical tube. Energy Sources Part a Recover Util Environ Eff 2023;45(3):7050–67. doi:10.1080/15567036.2023.2218306.
[24] Mishra I, Senapati P, Pandey M. Performance enhancement and comparison of inner-shielded solar parabolic trough collector with various nanoparticles in Syltherm-800 using computational fluid dynamics techniques. Clean Technol Environ Policy 2024. doi:10.1007/s10098-024-02942-8.